Diffractive phase-shift lithography photomask operating in proximity printing mode

Giuseppe A. Cirino[*1], Ronaldo D. Mansano[2], Patrick Verdonck[3], Lucila Cescato[4], and Luiz G. Neto[5]

[1] *CCET, Federal University of Sao Carlos, Rod. Whashington Luis, Km 235 - 13565-905, Sao Carlos, SP, Brazil*
[2] *PSI, University of Sao Paulo, Av. Prof. Luciano Gualberto, 158, trav. 3 - 05508-970, Sao Paulo, SP, Brazil*
[3] *IMEC, Kapeldreef 75, B-3001 Leuven, Belgium*
[4] *IFGW, Campinas State University, 13.083-970, Campinas, SP, Brazil*
[5] *EESC, University of Sao Paulo, Av. Trabalhador Sao-carlense, 400 - 13560-970, Sao Carlos, SP, Brazil*
** gcirino@ufscar.br*

Abstract: A phase shift proximity printing lithographic mask is designed, manufactured and tested. Its design is based on a Fresnel computer-generated hologram, employing the scalar diffraction theory. The obtained amplitude and phase distributions were mapped into discrete levels. In addition, a coding scheme using sub-cells structure was employed in order to increase the number of discrete levels, thus increasing the degree of freedom in the resulting mask. The mask is fabricated on a fused silica substrate and an amorphous hydrogenated carbon (a:C-H) thin film which act as amplitude modulation agent. The lithographic image is projected onto a resist coated silicon wafer, placed at a distance of 50 μm behind the mask. The results show a improvement of the achieved resolution – linewidth as good as 1.5 μm - what is impossible to obtain with traditional binary masks in proximity printing mode. Such achieved dimensions can be used in the fabrication of MEMS and MOEMS devices. These results are obtained with a UV laser but also with a small arc lamp light source exploring the partial coherence of this source.

OCIS codes: (310.6845) Thin film devices and applications; (070.7345) Wave propagation; (150.1135) Algorithms; (110.5220) Photolithography; (220.4000) Microstructure fabrication

References and links

1. M. D. Levenson, N. S. Viswanathan, and R. A. Simpson, "Improving resolution in photolithography with a phase-shifting mask," IEEE Trans. Electron. Dev. **29**(12), 1828–1836 (1982).
2. M.D. Levenson, "Using destructive optical interference in semiconductor lithography," Opt. Photon. News, 30-35 Apr. (2006).
3. M. D. Levenson, "Wavefront engineering for photolithography," Phys. Today 28–36, (1993).
4. M. D. Levenson, "Extending the lifetime of optical lithography technologies with wavefront engineering," Jpn. J. Appl. Phys. **33**(Part 1, No. 12B), 6765–6773 (1994).
5. M. Shibuya, "Projection master for transmitted illumination," Japanese Patent Gazette # Showa 62–50811, October 27, (1987).
6. G. Talor, "Transparent phase shift mask for fabrication of small feature sizes", US Patent 6 933 085 B1, August 23, (2005).
7. K. Kukuchi, US Patent Application US 2002/0177051 A1, "Phase shift mask, method of exposure, and method of producing semiconductor devices", August 03, (2002).
8. J. Turunen, and F. Wyrowski, in *Diffractive Optics for Industrial and Commercial Applications,* 1st.ed, (Berlin: Akademi. Verlag, 1997), Chap. 1.
9. D. C. O'Shea, T. J. Suleski, A. D. Kathman, and D. W. Prather, *Diffractive Optics: Design, Fabrication and Test*, (SPIE Press: Washington, 2004), pp. 115–121.
10. T. J. Suleski, W. F. Delaney, and M. R. Feldman, "Fabricating optical elements using a photoresist formed from proximity printing of a gray level mask", US Patent 6 638 667, October 28, 2003.
11. P. Dentinger, K. Krafcik, K. Simison, R. Janek, and J. Hachman, "High aspect ratio patterning with a proximity ultraviolet source," Microelectron. Eng. **61–62**, 1001–1007 (2002).
12. P. Canestrari, G. A. Degiorgis, P. de Natale, L. Gazzaruso, and G. Rivera, "Optimization of partial coherence for half-micron i–line lithography", in, IV Optical/Laser Microlithography," Proc. SPIE **1463**, 446–455 (1991).
13. D. Meyerhofer, and J. Mitchell, "Proximity printing of chrome masks," Polym. Eng. Sci. **23**(18), 990–992 (1983).

#130279 - $15.00 USD Received 17 Jun 2010; revised 6 Jul 2010; accepted 7 Jul 2010; published 20 Jul 2010

14. T. Lin, H. Yang, and C. Chao, “Concave microlens array mold fabrication in photoresist using UV proximity printing”, Symposium on Design, Test, Integration and Packaging of MEMS/MOEMS (DTIP’07), 11–15, (2007).
15. L. Ping, Y. Hsihamg, and C. Chao, “A new microlens array fabrication method using UV proximity printing,” J. Micromechan. Eng. **13**(5), 748–757 (2003).
16. H. Yang, C. K. Chao, T. H. Lin, and C. P. Lin, “Fabrication of microlens array with graduated sags using UV proximity printing method,” Microsyst. Technol. **12**(2), 82–90 (2005).
17. T. Lin, H. Yang, R. F. Shyu, and C.-K. Chao, “New horizontal frustum optical waveguide fabrication using UV proximity printing,” Microsyst. Technol. **14**(7), 1035–1040 (2008).
18. W. Henke, M. Weiss, R. Schwalm, and J. Pelka, “Simulation of proximity printing,” Microelectron. Eng. **10**(2), 127–152 (1990).
19. B. Meliorisz, and A. Erdmann, “Simulation of mask proximity printing”, J. Micro/Nanolithography, MEMS MOEMS **6**(2), 729–736 (2007).
20. B. Meliorisz, P. Evanschitzky, and A. Erdmann, “Simulation of proximity and contact lithography,” Microelectron. Eng. **84**(5), 733–736 (2007).
21. M. Teschke, and S. Sinzinger, “Novel approaches to the design of halftone masks for analog lithography,” Appl. Opt. **47**(26), 4767–4776 (2008).
22. S. A. Campbell, *The Science and Engineering of Microeledtronic Fabrication*, (Oxford University Press, 1996), Chap. 7.
23. H. Kirchauer, “Photolithography Simulation“, PhD. Dissertation, Fakultät für Elektrotechnik, Technischen, Universität Wien. (1998).http://www.iue.tuwien.ac.at/phd/kirchauer/
24. F. Wyrowski, E. Kley, T. J. Nellissen, L. Wang, and S. Bühling, “Proximity printing by wave-optically designed masks”, Proc SPIE **4436**, (2001).
25. S. Buhling, *et al*., “High resolution proximity printing by wave-optically designed complex transmission masks”, Proc SPIE **4404**, (2001).
26. L. G. Neto, R. D. Mansano, G. A. Cirino, L. S. Zambom, and P. Verdonck, “Amorphous hidrogenated carbon film”, US Patent 7,381,452, June (2008).
27. L. G. Neto, G. A. Cirino, R. D. Mansano, P. S. P. Cardona, and P. Verdonck, “Hybrid phase and amplitude modulation proximity printing mask fabricated on DLC and SiO2 substrates”, Proc SPIE **4984**, (2003).
28. L. G. Neto, P. S. P. Cardona, G. A. Cirino, R. D. Mansano, and P. Verdonck, “Design, fabrication, and characterization of a full complex-amplitude modulation diffractive optical element,” J. Microlithography, Microfabrication and Microsystems **2**(2), 96–104 (2003).
29. L. G. Neto, P. S. P. Cardona, G. A. Cirino, R. D. Mansano, and P. Verdonck, “Implementation of Fresnel full complex-amplitude digital holograms,” Opt. Eng. **43**(11), 2640 (2004).
30. G. A. Cirino, P. Verdonck, R. D. Mansano, and L. G. Neto, “Optical characterization of an amorphous-hidrogenated carbon film and its application in phase modulated diffractive optical elements” in *Proc. XVI International Conference on Microelectronics and Packaging*, Brazil, 140–145, (2001).
31. L. G. Neto, G. A. Cirino, R. D. Mansano, P. S. P. Cardona, and P. Verdonck, “Hybrid phase and amplitude modulation proximity printing mask fabricated on DLC and SiO2 substrates”, Proc SPIE **4984**, (2003).
32. J. W. Goodman, *Introduction to Fourier Optics*, 2nd ed., (McGraw-Hill, 1996), Chap. 3.
33. G. A. Cirino, R. D. Mansano, P. Verdonck, R. G. Jasinevicius, and L. G. Neto, “Diffraction gratings fabricated on DLC thin films,” Surf. Coat. Tech. **204**(18-19), 2966–2970 (2010).
34. C. R. A. Lima, L. L. Soares, L. Cescato, M. A. Alves, and E. S. Braga, “Diffractive structures holographically recorded in amorphous hydrogenated carbon (a-C:H) films,” Opt. Lett. **22**(23), 1805–1807 (1997).
35. L. L. Soares, *et al*., “Recording of relief structures in amorphous hydrogenated carbon (a-C:H) films for infrared diffractive optics,” J. Mod. Opt. **45**(7), 1479–1486 (1998).
36. L. G. Neto, L. B. Roberto, R. D. Mansano, P. Verdonck, G. A. Cirino, and M. A. Steffani, “Multiple Line Generation Over High Angle Using Hybrid Parabolic Profile and Binary Surface-Relief Phase Element,” Appl. Opt. **40**(2), 211–218 (2001).
37. R. D. Mansano, P. Verdonck, and H. S. Maciel, “Anisotropic reactive ion etching in silicon, using a graphite electrode,” Sens. Actuators A Phys. **65**(2-3), 180–186 (1998).
38. P. W. Leech, “Reactive ion etching of quartz and silica-based glasses in CF4/CHF3 plasmas,” Vacuum **55**(3-4), 191–196 (1999).
39. R. D. Mansano, “Effects of the methane content on the characteristics of diamond-like carbon films produced by sputtering,” Thin Solid Films **373**(1-2), 243–246 (2000).
40. S. A. Campbell, *The Science and Engineering of Microeledtronic Fabrication*, (Oxford University Press, 1996), Chap. 7.
41. P. Concidine, “Effects of coherence on imaging systems,” J. Opt. Soc. Am. **56**(8), 1001–1008 (1966).
42. M. Born, and E. Wolf, *Principles of optics: Electromagnetic theory of propagation, interference and diffraction of light*, 6th ed., (Pergamon, 1980), Chap. 10.
43. P. H. van Cittert, “Die wahrscheinliche Schwingungsverteilung in einer von einer Lichtquelle direct oder mittels einer Linse beleuchteten Ebene,” Physica **1**(1-6), 201–210 (1934).
44. F. Zernike, “The Concept of Degree of Coherence and Its Application to Optical Problems,” Physics **5**, 785–795 (1938).

#130279 - $15.00 USD Received 17 Jun 2010; revised 6 Jul 2010; accepted 7 Jul 2010; published 20 Jul 2010

1. Introduction

The huge importance of the lithography on the fabrication of micro devices is well known. For most applications binary photolithography masks are employed. These masks consist of a transparent plate, covered by a patterned opaque film that acts as a light intensity modulating agent. The phase shift mask technique, introduced in the beginning of the eighties, employs a transparent thin film that modulates the phase of the transmitted light in order to compensate the diffraction effect of the edges of the mask features [1–4]. This technique has been improved since then [5–7]. A phase shift of an incoming wavefront can be implemented both by adding a transparent thin layer with adjustable thickness on certain regions of the substrate, or by removing a specific amount of material from the same transparent region of the substrate. The first method imposes a π-phase delay in the wavefront, whereas the second one imposes a phase advancing by π radians. In this way, a phase shift mask can be considered a diffractive optical element capable of modulating both phase and amplitude (or intensity) of light [8–10].

Proximity printing has been a very popular lithographic technique for microelectronic fabrication, because of its simplicity and low cost. Although the resolution achieved by this technique is far too large for today's microelectronic fabrication, it is still very suitable for MEMS and MOEMS devices, with dimensions which typically range from several micrometers to several millimeters. Many authors have been exploring this technique, in several fields of MEMS and MOEMS applications. Dentinger and associates studied the influence on the final resolution for thick resists exposed in proximity mode [11]. Kathleen investigated modeling and characterization of the resolution of proximity printing x-ray lithography [12]. Meyerhofer and associates investigated the application of proximity printing in the copy of chrome masks, and shown its potential for replicating 10X step-and-repeat recticles [13]. The fabrication of microlens arrays by exploring the diffraction of light and proximity exposure has been demonstrated by Lin and associates [14], Ping and associates [15], and Yang and associates [16]. Lin and associates fabricated optical waveguides by this same technique [17]. Schwalm and associates have simulated the proximity printing lithography in a model, which takes into account the effects of wave propagation inside a resist layer, diffraction, standing waves and the profile degradation beyond certain limits for the proximity distance between mask and wafer [18]. Meliorisz and associates also presented simulation results for proximity printing lithography, and compared scalar with rigorous electromagnetic computations [19,20]. Teschke and associates have developed an interesting approach to implement halftone phase masks for analog lithography by using kinoform computer-generated holograms. This approach is derived from the interferometric phase contrast technique [21].

The resolution, W, of the proximity exposure technique is limited by the diffraction effects that occur at the mask pattern edges [22, 23], and given by

$$W = \gamma\sqrt{\lambda d_g} \tag{1}$$

where d_g denotes the gap between the mask and wafer under processing, λ is the operating wavelength and γ is a parameter which depends on the lithography process (typically $1< \gamma <2$).

Such square-root behavior of resolution degradation with respect to d_g, follows from the Fresnel diffraction theory, valid for near field observation behind the apertures of the mask [23]. Considering conventional optical lithography in proximity exposure mode, typical values are $\gamma = 1.6$, $\lambda = 0.4$ μm, and $d_g = 25$ μm, resulting in a resolution $W = 4$ μm.

The resolution of a lithography system operating in proximity printing mode can, however, be dramatically improved by replacing the conventional photo mask with a mask able to compensate the diffraction effects [10,24,25]. The final scale integration is also limited by the optical alignment errors of the different masks used during a micro device fabrication process. If a dark field photolithographic mask is necessary (e.g. to open holes for cantilever anchors with positive resist patterning), light is blocked over a wide region and the

#130279 - $15.00 USD Received 17 Jun 2010; revised 6 Jul 2010; accepted 7 Jul 2010; published 20 Jul 2010

optical alignment is a time consuming and relatively difficult operation. Another important point is that both the mask alignment task and the throughput can be improved if this mask blocks the light only in the UV region (< 400 nm), i.e., a mask that is partially transparent in the visible region of the spectrum (400 - 700 nm).

Wyrowski and associates [24,25] have presented a similar approach by designing wave-optically based complex transmission masks. They were able to resolve *3 μm* line/space patterns. The proximity mask used in their experiments was fabricated by e-beam lithography with four height levels and two amplitude transmission values.

In this work we propose a phase and intensity modulation diffractive phase shift proximity printing mask, fabricated using an amorphous hydrogenated (a:C-H) carbon thin layer - also known as Diamond-Like Carbon (DLC) - on top of a fused silica (SiO_2) substrate. The proposed diffractive structure was designed to form the required image within a plane at *50 μm* behind the mask, as shown in Fig. 1. In this figure the mask is located in the plane *(x',y',z=0)*, and the wafer under exposure is located in the plane *(x,y,z=50μm)*. This inter-plane distance may be chosen as most suited for the used alignment equipment. This gives another important degree of freedom for this procedure, optimizing the resolution of the transferred patterns for a specific equipment.

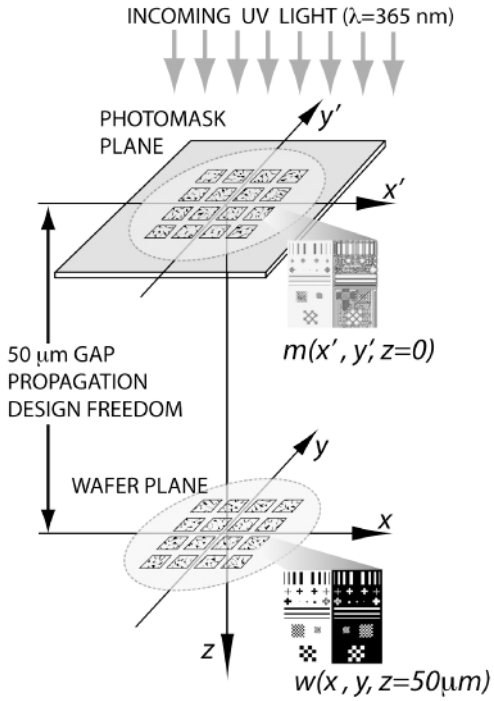

Fig. 1. Schematic view of the optical field projected by the mask, when illuminated by a UV plane wave. The pattern is obtained by applying free space light propagation along the 50 micrometers distance.

The photomask was fabricated by binary optics and a sub-cells-based coding scheme was introduced in order to increase the design degree of freedom: not restricted on four phase levels or two amplitude levels. Another novelty of this work is the employment of an a:C-H thin film to modulate the light amplitude. The mask is designed to operate in low cost aligners, where transparent masks facilitate a lot the alignment process of the relatively poor optical system of the aligner, e.g. for a situation where a dark field mask needs to be used to transfer small sparse regions to a wafer. The proposed mask would ease the alignment task of structures over the whole wafer, i.e. structures very far apart with a large rotation

#130279 - $15.00 USD Received 17 Jun 2010; revised 6 Jul 2010; accepted 7 Jul 2010; published 20 Jul 2010

misalignment. This alignment is much more complicated in a situation where the light is blocked by a metal opaque film, even in a complex-amplitude transmittance photomask.

The amorphous carbon layer blocks the light only in the UV region, being partially transparent in the visible region of the spectrum. This characteristic makes mask alignment much easier. The choice of this material is based on previous results [26–30]. When illuminated, the mask projects the required pattern at a predetermined distance by the modulation of both phase and amplitude of the UV exposure beam. The fused silica is used to modulate the phase and the a:C-H layer to modulate the intensity of the incoming UV light plane wave [31].

2. Design of the diffractive photomask

To generate the optical reconstruction, the scalar diffraction theory was employed [32], by considering the free space propagation of the light along the gap between mask and wafer planes. The mask has been designed bythe inverse propagation of light [28,29,31]. In this method, the desired complex distribution of the mask *m(x',y',z=0) = w(x',y', z=0)* is obtained by solving the Helmholtz equation $(\nabla^2 + k^2)w(x, y, z) = 0$ in the frequency domain [32] for a predefined intensity light distribution *w(x,y, z=50μm)*, which must be present in the wafer plane, Fig. 1.

A coherent light wavefront (at *365 nm* wavelength) is traveling with a component of propagation in the positive *z* direction, perpendicular to the *(x,y)* plane. The goal is to calculate the distribution *m(x',y', z=0),* at the *(x',y')* plane located at the coordinate *z=0*, as a function of *w(x,y, z=50μm)* at the *(x,y)* plane, located at the coordinate *z=50 μm.* This distance was chosen due to the requirement that the light wavefront must propagate a minimum distance in order to effectively explore the diffraction phenomena. Furthermore, the *50 μm* gap can be easily set in virtually all exposure tools.

If the relation between the light distribution *w(x,y, z=50μm)* and *m(x',y', z=0)* is found in the frequency space, then the diffraction effects of the light propagation will form the desired image. Additionally *w(x,y, z=50 μm)* must satisfy the Helmholtz equation. In this analysis it is necessary to introduce the functions $W(f_x,f_y, z=50\mu m)$ and $W(f_x,f_y, z=0) = M(f_x,f_y, z=0)$ as the two-dimensional Fourier Transform of the functions *w(x,y, z=50μm)* and *m(x',y', z=0)*, respectively; f_x and f_y are the frequency coordinates in the *x* and *y* directions, respectively.

The application of the requirement above shows that $W(f_x,f_y, z=50\mu m)$ must satisfy the differential equation [32]:

$$\frac{\partial^2}{\partial z^2} W\left(f_x, f_y, z\right) + \left(\frac{2\pi}{\lambda}\right)^2 \left[1 - \left(\lambda f_x\right)^2 - \left(\lambda f_y\right)^2\right] W\left(f_x, f_y, z\right) = 0 \qquad (2)$$

An elementary solution of this equation, in the frequency space, can be written in the form:

$$W\left(f_x, f_y, z\right) = M\left(f_x, f_y, 0\right) \exp\left[j \frac{2\pi}{\lambda} z \sqrt{1 - \left(\lambda f_x\right)^2 - \left(\lambda f_y\right)^2} \right], \; j = \sqrt{-1} \qquad (3)$$

From the above result, the propagation phenomenon may be regarded as a linear, dispersive spatial filter with a finite bandwidth of extension inside a circular region with radius λ^{-1} in the frequency plane. Its transfer function, $H(f_x,f_y)$, is given by

$$H\left(f_x, f_y\right) = \begin{cases} \exp\left[j \frac{2\pi}{\lambda} z \sqrt{1 - \left(\lambda f_x\right)^2 - \left(\lambda f_y\right)^2} \right] & \text{for} \quad \sqrt{\left(f_x\right)^2 + \left(f_y\right)^2} < \frac{1}{\lambda} \\ 0 \quad \text{otherwise} \end{cases} \qquad (4)$$

Figure 2 shows a schematic diagram of the phenomenon of free space propagation, and its relation with frequency and image spaces, as well as mask and wafer planes.

#130279 - $15.00 USD Received 17 Jun 2010; revised 6 Jul 2010; accepted 7 Jul 2010; published 20 Jul 2010

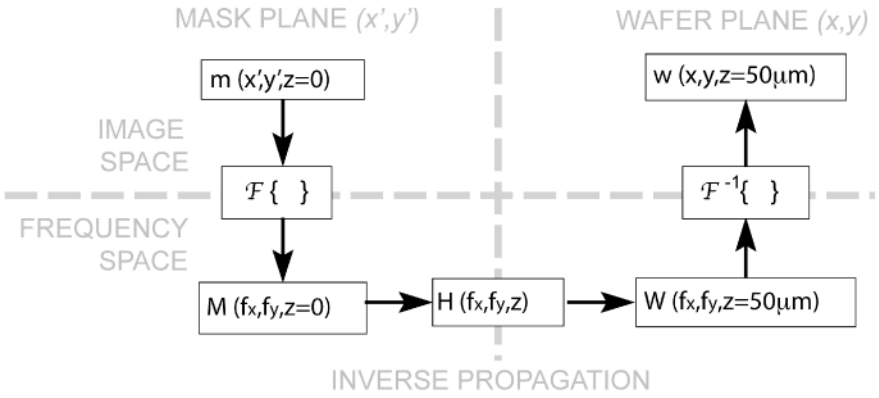

Fig. 2. Schematic diagram of the phenomenon of free space propagation, and its relation with frequency and image spaces, as well as mask and wafer planes.

Equation (3) describes, in the frequency space, the relation between the desired light distribution in the wafer plane *w(x,y,z=50μm)* and the diffraction structure in the mask plane, *m(x',y',z=0)*. To calculate the inverse propagation from the wafer plane to the mask plane, one has to apply the inverse filter for propagation:

$$m(x', y', z=0) = \Im^{-1}\left\{ \frac{W\left(f_x, f_y, z=50\mu\text{m}\right)}{\exp\left[j\frac{2\pi}{\lambda} z\sqrt{1-\left(\lambda f_x\right)^2-\left(\lambda f_y\right)^2}\right]} \right\} \tag{5}$$

where $\Im\{.\}$ denotes the two-dimensional Fourier Transform operator.

Figure 3 shows a schematic view of the basic algorithm used for the calculations of the proposed diffractive mask. It consists in generating a complex-valued distribution by performing the propagation path backwards (inverse propagation). Afterwards this complex-valued distribution is mapped into a suitable set of photolithographic masks by applying a coding scheme, as detailed in section 3.

The algorithm is initiated by establishing the desired image intensity distribution at the wafer plane, *w(x,y,z=50μm)*. Then the inverse light propagation back to the mask plane is performed in the frequency space, generating a complex distribution, which can be written as an amplitude and a phase distribution. The obtained amplitude and phase information may be used in the fabrication of the diffractive phase shift photomask.

In the calculation of the inverse light propagation, the following normalized function, $m_N(x',y')$, is considered [30–32],

$$m_N\left(x', y'\right) = \beta\, m\left(x', y'\right) = A\left(x', y'\right)\exp\left[j\phi\left(x', y'\right)\right] \tag{6}$$

#130279 - $15.00 USD Received 17 Jun 2010; revised 6 Jul 2010; accepted 7 Jul 2010; published 20 Jul 2010

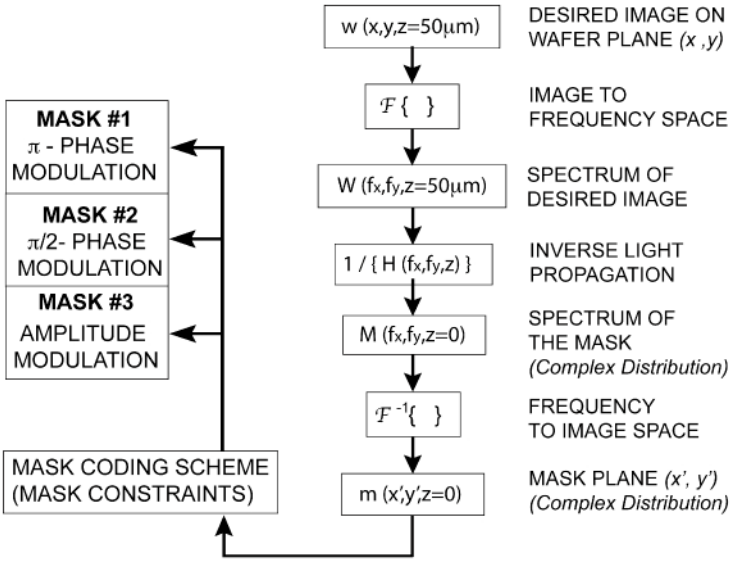

Fig. 3. Schematic view of the basic algorithm used for the calculations of the proposed phase shift diffractive photomask. The inverse propagation is computed and the resulting complex-valued distribution is mapped into three photolithographic masks.

where $A(x',y') = |m(x',y')|$ is the amplitude $[0 \le A(x',y') \le 1]$, $\phi(x',y')$ is the phase distribution $[0 \le \phi(x',y') \le 2\pi]$, $\beta=\{\text{MAX}\,[m(x',y')]\}^{-1}$ is a scale factor (a real number) used to normalize the maximum amplitude of $|m(x',y')|$ to unity, and the operator MAX[.] represents the maximum value of the function $m(x',y')$. In the design, the desired reconstruction is a real distribution $w(x,y,z=0) = |w(x,y,z=0)| \exp[j0]$.

Figure 4a shows the intensity distribution of a test structure desired to be transferred to the wafer, $w(x,y,z=50\mu m)$; Figs. 4b and 4c show the corresponding amplitude distribution, $A(x',y')$ $[0<A<1]$, and phase distribution, $\phi(x',y')$ $[0<\phi<2\pi]$, to be implemented in the mask after applying the propagation method described above.

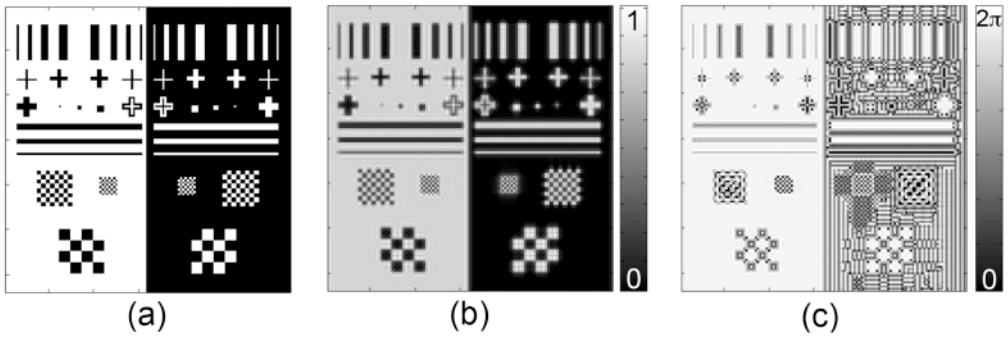

Fig. 4. Lithographic test structures used to show the basic idea of the complex-amplitude modulation proximity printing mask (a) Numerical reconstructed image of the desired light distribution; (b) amplitude $A(x',y')$ and (c) phase $\phi(x',y')$ distributions of the resulting phase shift photomask.

3. Diffractive mask coding scheme

The resulting inverse light propagation normalized distribution, $m_N(x',y')$, calculated from the desired light distribution $w(x,y)$, with values of both phase and amplitude, must be coding in the mask plane (x',y'). From a computer holography point of view, it is convenient to represent the functions in the mask and wafer planes as an array of discrete sampled values.

#130279 - $15.00 USD Received 17 Jun 2010; revised 6 Jul 2010; accepted 7 Jul 2010; published 20 Jul 2010

Considering these functions as band limited, i.e., functions whose Fourier Transforms are non-zero over only a finite region in frequency space, the reconstruction can be obtained exactly, providing the interval between samples is smaller than a certain value, as stated by the Whittaker-Shannon sampling theorem [28,29].

The continuous phase distribution can be implemented using variable dose electron beam lithography, or a laser ablation process, generating a continuous variation in the thickness of a suitable optical quality glass [30–32]. In this work, however, considering the time and cost involved in a process that generates continuous phase profiles, it is proposed to use the so-called binary optics method [21,22,33,34] for the fabrication of the phase shift diffractive photomask. In this method of fabrication, both the phase and amplitude information (which are continuous distributions) are approximated by a stepwise approach. To this end, a set of conventional binary photolithographic masks is fabricated from the continuous information by a search and sampling algorithm. Once the mask set is obtained, the phase shift diffractive photomask can be fabricated. The characteristics and number of photolithographic masks depends on the number of level approximation and the coding scheme used to map the phase and amplitude information.

The mask consists of several test structures, with *128×128* cells. Each cell contains 16 sub-cells, in a *4×4* arrangement. The total size of the test structures (each chip of the photomask) is *2.56 mm*. As shown in Fig. 3, the phase distribution, $\phi(x',y')$, is sampled to yield four phase delaying levels: *0, π/2, π*, and *3π/2* radians. The amplitude distribution, $A(x',y')$, is sampled to yield five possible values: *0, 25, 50,75* and *100%* of the total cell size. Mask #1 will create a *π/2*-phase delay profile and mask #2 a *π*-phase delay profile. Combining these two masks it is possible to create the desired relief in the optical substrate, with four levels discretization. To implement the amplitude modulation, an opaque layer is deposited on top of the transparent substrate with the four-level phase relief, and patterned by a third lithographic mask (mask #3). The amplitude modulation is achieved by removing small parts of the opaque layer over the region of each phase pixel structure previously patterned. These apertures act as local diaphragms controlling the desired light transmission, in such a way that the dimension of these apertures must be proportional to the amplitude $A(x',y')$.

A representation in the complex plane of all possible values of amplitude and phase considering the above coding scheme is shown in Fig. 5. The four possible values of phase are represented in Fig. 5a, by four points over the imaginary and real axes of the complex plane, with a distance equals to unity from the origin. The amplitude modulation can be represented by a segment over the positive real axe in Fig. 5b, which can have five possible magnitude values between *0* and *1*, being proportional to the open area of an opaque thin layer as explained above. Figure 5c shows the combination of the previous two representations.

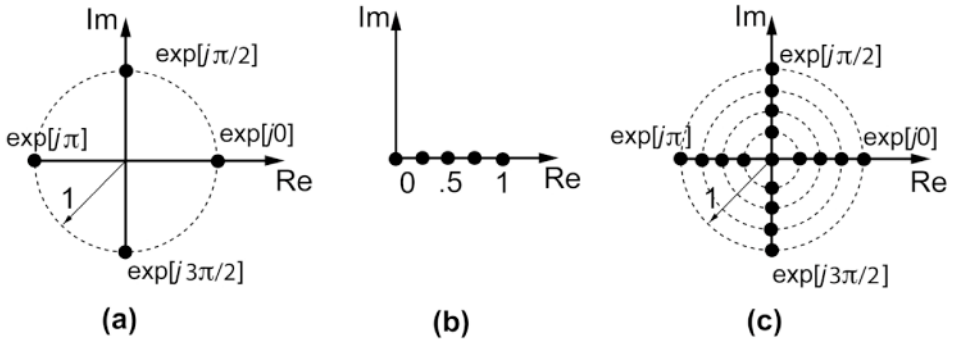

Fig. 5. Schematic representation in the complex plane of possible values of amplitude and phase considering (a) four phase-levels sampling; (b) five amplitude-levels sampling; (c) combination of previous values of phase and amplitude.

#130279 - $15.00 USD Received 17 Jun 2010; revised 6 Jul 2010; accepted 7 Jul 2010; published 20 Jul 2010

In order to give additional degree of freedom and expand the possible values attributed to the functions $\phi(x',y')$ and $A(x',y')$, consider the cells of the photomask shown in Fig. 6. The cell centers are spaced at regular intervals of width X in the x' direction and regular intervals of width Y in the y' direction. Since each cell is divided in sub-cells, it is possible to deal with the relation between areas that assume two different values of phase and/or amplitude inside this cell. Consider, for example, the first quarter of complex plane [30–32]. Figure 6 illustrates the subdivision of a cell, formed by 4×4 sub-cells, with new possible values of phase and amplitude.

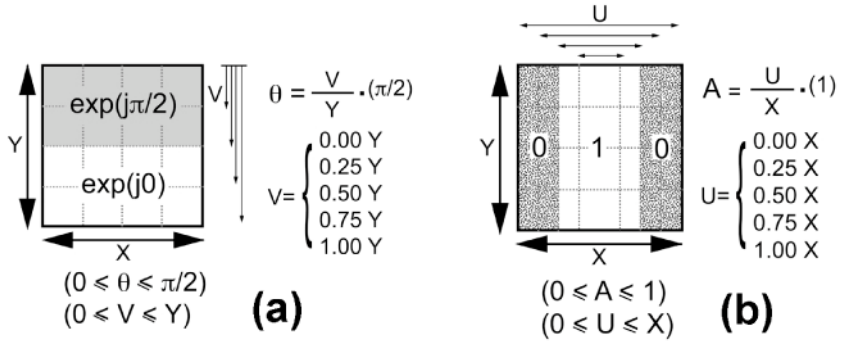

Fig. 6. Subdivision of a cell, formed by 4 × 4 sub-cells. (a) structure of a particular cell that can modulate the phase between *0* and *π/2*, depending of the value of *V*; (b) structure of a window created over the phase cell of Fig. 9a, in order to modulate the amplitude of incident light between 0 and 1, depending of the value of *U*.

Figure 6a shows the structure of a particular cell that can modulate the phase between *0* and *π/2*. Intermediate phase values of the function $\phi(x',y')$, distributed between *0* and *π/2*, can be approximated by combining different regions inside the cell. The variation of *V*, from *0* to *Y* inside the cell will introduce a smooth phase variation from *0* to *π/2* radians. Figure 6b shows the structure of a window created on top of the phase cell of Fig. 6a, in order to modulate the amplitude of incident light between *0* and *1*. The variation of *U*, from *0* to *X* inside the cell will introduce a smooth amplitude variation from *0* to *1*.

Figure 7a shows the structure of a particular cell with complex transmittance of amplitude equal to *0.5* and phase equal to *π/4*. Figure 7b shows all the possible values (black dots) of amplitude and phase within the first quadrant, as well as, the particular value of the cell of Fig. 7a. The full complex-amplitude modulation is achieved on the entire complex plane, i.e., on the regions of second, third and fourth quadrant, by combining, respectively, phase values *π/2-π*, *π-3π/2*, and *3π/2-0*.

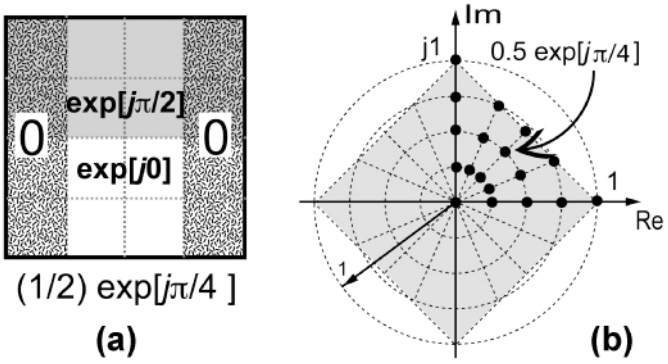

Fig. 7. (a) Structure of a particular cell with complex transmittance of amplitude equal to 0.5 and phase equal to *π/4*; (b) all the possible value (black dots) of amplitude and phase within the first quadrant, as well as, the particular value of the cell of figure (a).

#130279 - $15.00 USD Received 17 Jun 2010; revised 6 Jul 2010; accepted 7 Jul 2010; published 20 Jul 2010

4. Diffractive mask structure and error analysis

The diffractive phase shift mask is considered as a two-dimensional matrix structure with $M \times N$ rectangular cells of dimensions $X \times Y$, with M and N being even numbers. Each cell represents a complex transmittance value $m_{kl}(x',y')$ with $[(-M/2) \le k \le ((M/2)-1)]$ and $[(-N/2) \le l \le ((N/2)-1)]$.

The phase and amplitude information must be mapped into the discrete values:

$$A(x',y')\exp\left[j\phi(x',y')\right] \leftrightarrow A_{kl}(x',y')\exp\left[j\theta_{kl}(x',y')\right] \tag{7}$$

Considering the cell structure described above and supposing that the mask is placed in the (x',y') plane, one has:

$$m_{kl}(x',y') = rect\left(\frac{x'}{MX},\frac{y'}{NY}\right)\left\{\sum_{k=-M/2}^{M/2-1}\sum_{l=-N/2}^{N/2-1} rect\left(\frac{x'-kX}{A_{kl}}\right)\left[\begin{array}{l} rect\left(\dfrac{y'-lY}{Y}\right)+ \\ \left(e^{j\pi/2}-1\right) rect\left(\dfrac{y'-Y\left(\dfrac{1}{2}-\dfrac{\theta_{kl}}{\pi}\right)-lY}{Y-\dfrac{2\theta_{kl}}{\pi}}\right)\end{array}\right]\right\} \tag{8}$$

The errors introduced by approximating the full complex distribution $A(x',y').exp[\phi(x',y')]$ using the cell structure of Fig. 6 can be analyzed in the frequency plane, by calculating the Fourier transform of Eq. (8):

$$M_{kl}(f_x,f_y) = \sin c\left(MXf_x, NYf_y\right)\otimes$$
$$MNXY^2\left\{\sum_{k=-M/2}^{M/2-1}\sum_{l=-N/2}^{N/2-1} A_{kl}\sin c\left(A_{kl}f_x\right)e^{-j2\pi kXf_x}\left[\begin{array}{l}\sin c\left(Yf_x\right)e^{-j2\pi lYf_y}+\dfrac{2\theta_{kl}}{\pi}\left(e^{j\pi/2}-1\right)\times \\ \sin c\left(Y\dfrac{2\theta_{kl}}{\pi}f_y\right)e^{-j2\pi Y(1/2-\theta_{kl}/\pi)f_y}e^{-j2\pi lYf_y}\end{array}\right]\right\} \tag{9}$$

where $sinc(a,b) = sinc(a) \times sinc(b)$ and $\otimes$ denotes the convolution operation. In Eq. (9) the function $M_{kl}(f_x,f_y)$ can be sampled with intervals R in the f_x direction $[f_x=mR;\ R=1/(MX)]$ and S in the f_y direction $[f_y=nS;\ S=1/(NY)]$. During the calculation of the free space propagation using Eq. (3), the region of interest of $M_{kl}(f_x,f_y)$ in the frequency plane is much smaller than the width of the *sinc* functions, which can be replaced by unity inside this region. This is a valid approximation considering that in the design, the desired reconstruction is a real distribution $f(x,y,0)=|f(x,y,0)|\,exp[j0]$, and is almost all concentrated in the center of the region $[(-8/MX,+8/MX);(-8/NY,+8/NY)]$ of the frequency plane. The resulting approximation can be written by

$$M_{kl}(f_x,f_y) = \sin c\left(MXf_x, NYf_y\right)\otimes$$
$$MNXY^2\left\{\sum_{k=-M/2}^{M/2-1}\sum_{l=-N/2}^{N/2-1} A_{kl}\left[1+\frac{2\theta_{kl}}{\pi}\left(e^{j\pi/2}-1\right)e^{-j2\pi(1/2-\theta_{kl}/\pi)n/N}\right]e^{-j2\pi(mk/M+nl/N)}\right\} \tag{10}$$

One further approximation can be done. In the center of the region $[(-8/NY,+8/NY)]$ the following maximum phase factor value

$$2\pi\left(\frac{1}{2}-\frac{\theta_{kl}}{\pi}\right)Yf_y = 2\pi\left(\frac{1}{2}-\frac{\theta_{kl}}{\pi}\right)\frac{n}{N} \tag{11}$$

is assumed to be equal to $\pi/16$ for $\theta_{kl}=0$ and $N=128$. In this case, the exponential term $exp[-i2\pi\,(1/2-\theta_{kl}/2)] \approx 1$, leaving the following expression for $M_{kl}(f_x,f_y)$:

#130279 - $15.00 USD Received 17 Jun 2010; revised 6 Jul 2010; accepted 7 Jul 2010; published 20 Jul 2010

$$M_{kl}\left(f_x, f_y\right) = \sin c\left(MXf_x, NYf_y\right) \otimes$$
$$MNXY^2 \left\{ \sum_{k=-M/2}^{M/2-1} \sum_{l=-N/2}^{N/2-1} A_{kl} \left[1 + \frac{2\theta_{kl}}{\pi}\left(e^{j\pi/2} - 1\right)\right] e^{-j2\pi(mk/M + nl/N)} \right\} \quad (12)$$

In Figs. 6a and 7a the variation in the area of the regions that modulate the phase 0 and the phase $\pi/2$ results in the complex term $1+(2\theta_{kl}/\pi)$ $[exp(j\pi/2)-1)]$, shown in Fig. 7b [29]. This error is calculated considering the maximum normalized value of amplitude equal to unity. This term introduces a visible coupled amplitude modulation error ae_{kl} [29]:

$$ae_{kl} = \left| 1 + \frac{2\theta_{kl}}{\pi}\left(e^{j\pi/2} - 1\right)\right|. \quad (13)$$

The phase error introduced by this term pe_{kl} is given by the difference between the desired phase value and the argument of Eq. (13):

$$pe_{kl} = \left| \theta_{kl} - arg\left[1 + \frac{2\theta_{kl}}{\pi}\left(e^{j\pi/2} - 1\right)\right]\right|. \quad (14)$$

Verifying the above equation, one finds that the maximum value of pe_{kl} is achieved when $\phi_{kl} = \pi/8$ and $\theta_{kl} = 3\pi/8$, i.e. the $max[pe_{kl}] = 0.07\ rad$ for $0 \le \theta_{kl} \le \pi/2$. Considering this small value, the phase error can be neglected, resulting in the relation

$$\theta_{kl} = \phi\left(kX, lY\right). \quad (15)$$

Since the five-value amplitude modulation is achieved by varying the width A of the rectangular aperture $A \times Y$ created over each four-value phase structure, the resulting full complex-amplitude modulation is shown as the gray area of the normalized complex plane in Fig. 7b, with the coupled amplitude error modulation introduced by the variation of A. In Eq. (13), the minimum value of ae_{kl} cause by this coupled amplitude error, is achieved when $\theta_{kl} = \pi/4$, i.e $min[ae_{kl}] = 2^{1/2}/2$ for $0 \le \theta_{kl} \le \pi/2$. In this manner, the corrected value A_{kl} for the desired amplitude modulation $a(kX,lY)$ is determined by [29]

$$A_{kl} = \frac{\sqrt{2}}{2} \frac{a\left(kX, lY\right)}{ae_{kl}}. \quad (16)$$

The previous analysis shows that the phase structure suggested in Fig. 7 is a good approximation to encode the desired full complex-amplitude diffractive photomask. A similar error analysis can be extended to the second, third and fourth quadrant of the complex plane by combining, respectively the $\pi/2-\pi$, $\pi-3\pi/2$ and $3\pi/2-0$ phase values with the apertures $U \times Y$ created over each phase structure.

5. Fabrication of the phase shift photomask

The phase shift diffractive photomask must be implemented using the discrete phase and amplitude information. The phase distribution was transferred by generating a variation of the thickness $d_{kl}(x',y')$ on a fused silica substrate with refractive index n_{SiO2}, using the relation

$$d_{kl}(x', y') = \frac{\theta_{kl}(x', y')}{2\pi} \frac{\lambda}{(n_{SiO2} - 1)} \quad (17)$$

where $\lambda = 365nm$ is the operating wavelength of the exposure light source.

This variable thickness was approximated by using binary optics [9], with four phase-levels as shown in Fig. 3. To implement the amplitude modulation in this phase shift diffractive mask, an a:C-H layer is deposited on top of the SiO_2 four-level phase relief, and patterned by a third lithographic mask (mask #3), generating the variable apertures size over

#130279 - $15.00 USD Received 17 Jun 2010; revised 6 Jul 2010; accepted 7 Jul 2010; published 20 Jul 2010

the region of each phase pixel structure previously patterned. It should be mentioned that this carbon layer is opaque at $\lambda = 365\ nm$, and relatively transparent in the visible region of the spectrum.

In order to determine a good intensity light modulation process, a:C-H films of different thicknesses were deposited upon blank fused silica wafers and their optical transmittance was quantified employing the UV-Vis-NIR spectrometric technique (equipment model Carry 500 from Varian Co.). A good thickness was found to be *1500 nm*.

Initially a bare fused silica substrate was submitted to the transmittance spectral measurement. Afterwards, on top of this same substrate an a:C-H layer was deposited and this sample was submitted to the transmittance spectral measurement.

Figure 8 shows the optical transmittance of a *1500 nm* thick a:C-H thin film, as well as the transmittance of the respective fused silica substrate.

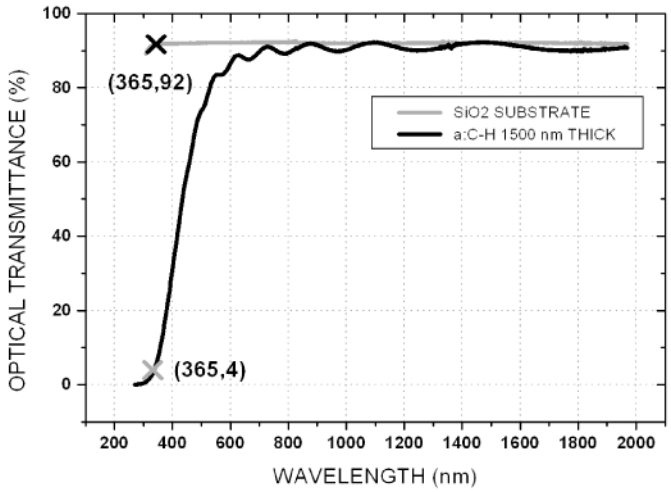

Fig. 8. Optical transmittance of a 1500 nm thick a:C-H thin film (black), and a fused silica substrate (gray). The thin film presents 4% transparency at exposure wavelength, while being partially transparent in the visible region.

One can note the flat transmittance behavior of the bare substrate at 92%. The 8% loss is due to refractive index mismatch between air and the fused silica substrate. Considering the sample with the presence of the carbon thin film, there is a strong absorption in the UV spectral region due to the a:C-H layer and the transmittance is only 4% at the operating wavelength. This opacity degree is enough to implement an intensity modulation in the photomask.

The transmittance uniformity along the 3-inch wafer is better than 97%, as measured among several points along the wafer including the center, border and halfway between center and border. Considering the exposure wavelength of *365 nm*, a *1500 nm* thick a:C-H layer blocks almost all the incoming light, while at the visible region of the spectrum this same layer is relatively transparent. This characteristic of semi-transparency in the visible region enables an easier alignment between different masks, certainly for dark field masks.

The carbon thin film was deposited by reactive magnetron sputtering [26, 36], employing a high purity graphite electrode. The deposition condition was as follows: a *70 sccm* methane flow rate, *5 mTorr* pressure and *150* W_{RF} power. At these process conditions a deposition rate of *16 nm/min* was obtained.

Atomic Force Microscopy (AFM) measurements showed that the RMS roughness of a *1500 nm* thick layer was *2.5 nm* when deposited over the fused silica substrate. Even after a reactive ion etching of a *600 nm* deep trench on the a:C-H film, the resulting RMS roughness was *4.7 nm* (meaning a roughness less than $\lambda/75$) [33].

#130279 - $15.00 USD Received 17 Jun 2010; revised 6 Jul 2010; accepted 7 Jul 2010; published 20 Jul 2010

Figure 9 shows schematically the entire process to fabricate the proposed diffractive phase shift proximity photomask. The first step etches the fused silica substrate anisotropically in order to obtain an etch depth which generates a phase delay of $\pi/2$ (mask #1), i.e. an etch depth of $d\#1 = \lambda.[4(n_{SiO2} - 1)]^{-1}$.

The refractive index of the fused silica substrate is $n_{SiO2} = 1.45$, and $\lambda = 365nm$, so the etch depth of the first etching process $d\#1 = 365.[4(1.45-1)]^{-1} = 209\ nm$. In the second step, the etch depth must be doubled, i.e. $d\#2 = \lambda.[2(n_{SiO2} - 1)]^{-1} = 418\ nm$.

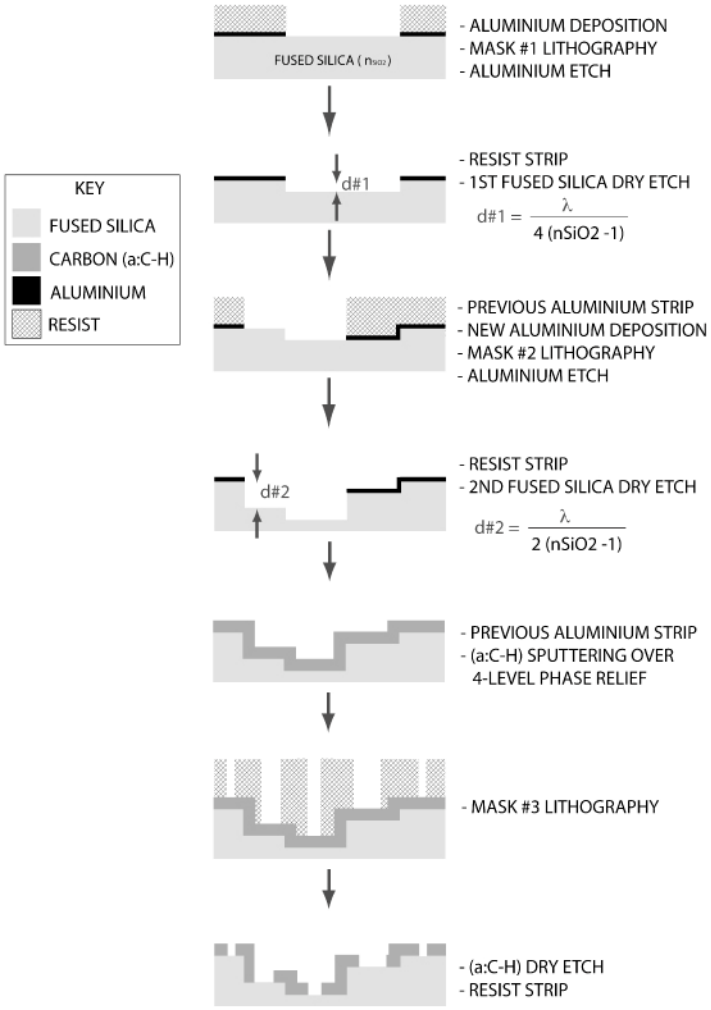

Fig. 9. Schematic view of the entire process to fabricate the proposed diffractive phase shift proximity photomask.

The total amplitude relief of one-lambda phase modulation in fused silica is $\lambda.[(n_{SiO2} - 1)]^{-1} = 811\ nm$, which means a proportion to the *1500 nm* thick carbon layer of 54%. Although the a:C-H film is almost twice thicker than the phase structure maximum height relief, previous work showed that it can be etched very anisotropically in an oxygen-based plasma enabling sharp sidewalls [33]. It is possible to pattern much better and deeper lamellar structures in a:C-H than in fused silica. Well-defined lamellar structures with aspect ratio of 2 can be obtained in carbon films [34,35].

A 3-inch diameter fused silica substrate was firstly cleaned with an ammonium hydroxide solution, then rinsed and dried. Upon this substrate, a *150 nm*-thick aluminum layer was

#130279 - $15.00 USD Received 17 Jun 2010; revised 6 Jul 2010; accepted 7 Jul 2010; published 20 Jul 2010

thermally evaporated to serve as a mask for the first plasma-etching step. Then a photo resist layer was spun coated at *2000 rpm* during *20 s* and submitted to a soft bake at *105°C* during *90 s*. The sample was exposed to UV light in order to transfer the $\pi/2$ phase delay mask pattern (mask #1), followed by the development step and hard bake at *115°C* during *5 min*.

The aluminum was wet etched in a solution of $10H_3PO_4$ + $1HNO_3$ + $5H_2O$-DI, during *8 min*. The remaining photoresist was then removed in an acetone bath at *70°C*, followed by an isopropyl alcohol immersion at the same temperature.

The fused silica substrate was then plasma etched [36] in a home built Reactive Ion Etching (RIE) system [37], using the following process conditions: *50 mTorr* chamber pressure, *60* W_{RF} power (*0.33* W/cm^2), using CF_4 gas (*20 sccm* flow rate). With these process conditions, an etch rate of *15.4 nm/min*, with a cathode self-bias of *400*V_{DC}, was obtained. After the plasma etching process, the aluminum layer was removed in the same phosphoric acid based solution as mentioned above, and the sample was again cleaned in an ammonium hydroxide solution, rinsed and dried. At this point the sample was ready to receive the second plasma etching step sequence, as shown in Fig. 9. All the process steps are the same as for the first fused silica patterning step, except that now the π-phase delay mask (mask #2) was employed, and the etching time was doubled to *26 min*, concluding the four phase-levels structure.

The pattern transfer from masks #1 and #2 to fused silica substrate employing dry etching process based on CF_4 chemistry was not perfect. There are some imperfections, mainly at the corners of the structures, with size of the order of *0.2* μm, which eventually will propagate into the final structures to be patterned. It has also been reported that the etching of fused silica substrates is not as easy and as reproducible as that of silicon wafers [38]. During our investigations, we observed similar problems, hence a pure CF_4 plasma etching process was chosen, requiring the use of an aluminum mask. Despite the induced line edge roughness, it is possible to demonstrate the proposed principle as explained in the results section.

A *1500 nm* thick a:C-H layer was then reactive sputter deposited on top of the four-level phase structure on the fused silica substrate, after which the sample was patterned by the amplitude modulation mask (mask #3). In order to open the windows with areas proportional to the transmitted light amplitude, the a:C-H layer was anisotropically etched using the same etching chamber as for the phase structures' etching, using the following process conditions: *20 sccm* of oxygen, *50 mTorr* pressure, *100* W_{RF} power (*0.55* W/cm^2). With these process conditions, an etch rate of *300 nm/min*, with a cathode self-bias of *520* V_{DC} was obtained, with a selectivity of approximately 1:1 with respect to the resist mask. With this process the exposed a:C-H film was etched without affecting the fused silica substrate below. The remaining photoresist layer was then removed as after the earlier etching steps. A final rinse in de-ionized water was performed finishing the fabrication of the device.

Figure 10a shows a photo of the fabricated phase shift diffractive photomask on a 3-inch fused silica wafer; Fig. 10b shows an overview the whole test structure.

The quality of the pattern transferred to the a:C-H film is much better than that of the fused silica pattern. AFM characterization showed no imperfections for this film, after reactive ion etching process. This indicates that the main problem of the manufacturing of the mask is in the plasma etching of the fused silica substrate, as could be expected.

#130279 - $15.00 USD Received 17 Jun 2010; revised 6 Jul 2010; accepted 7 Jul 2010; published 20 Jul 2010

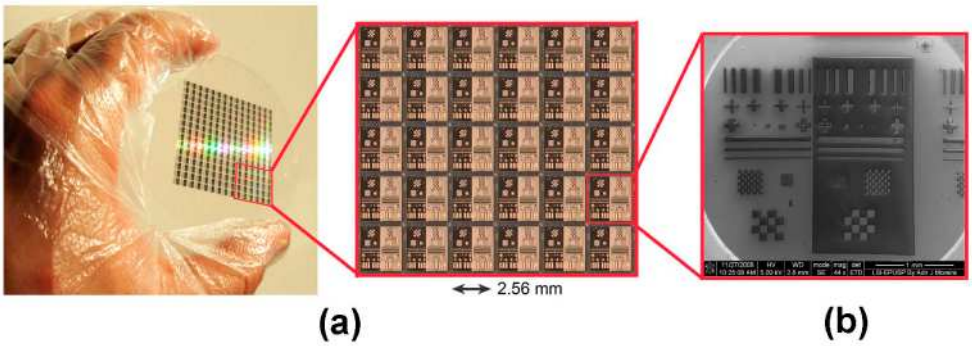

Fig. 10. (a) Photography of the fabricated phase shift diffractive photomask on a 3-inch fused silica wafer. The zoom in shows the whole test structure; (b) SEM picture of the whole test structure.

6. Exposure of the diffractive photomask into photo resist

In order to demonstrate the principle of the diffractive phase shift proximity printing photomask, the test structures shown in Fig. 4a were exposed on a silicon substrate by coherent argon-ion laser UV light operating at *368.3 nm* wavelength - the most near wavelength used in the design (*365 nm*). The test consists in comparing the exposure results from contact and proximity (*50 μm* gap) mode, with all the other parameters kept constant.

A schematic view of the experimental setup is shown in Fig. 11. The gap between mask and wafer under exposure was formed by using a *50 μm* thick spacer. The laser source used was a *5W*, multiline argon ion laser, model 2020 from Spectra Physics, operating at *363.8 nm*. A prism was used to separate this line. After being filtered and expanded, the beam power density was approximately *10 mW/cm*^{2}.

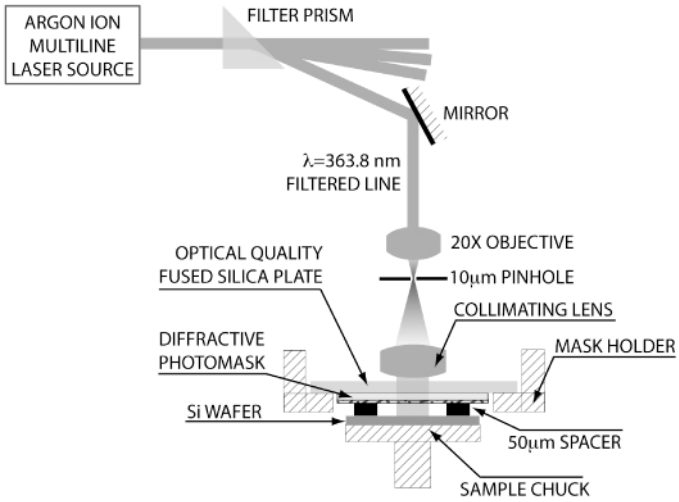

Fig. 11. Schematic view of the experimental setup used to perform the exposure with a coherent, multiline argon laser.

A photoresist layer with *1.2 μm* thickness was exposed during *32 s* by the incoming laser UV beam, followed by the development step. Figure 12 shows SEM images of the resulting structures from the two kinds of coherent light exposure: contact and proximity modes.

The structures obtained from the proximity printing mode exposure are much more clearly resolved than those obtained from the contact mode. This result indicates that the light propagation through the distance of *50 μm* is a necessary condition to obtain the maximum resolution with the used mask, contrary to what is observed when using traditional binary

#130279 - $15.00 USD Received 17 Jun 2010; revised 6 Jul 2010; accepted 7 Jul 2010; published 20 Jul 2010

lithography masks, where contact printing always results in better resolution than proximity printing.

It is possible to note also the strong speckle pattern due to the use of highly coherent argon-ion laser light in the exposure. Excimers emit strongly in a multimode fashion with a relatively poor spatial coherence. This is a strong drawback for many lasers applications, but it is actually an advantage for lithography. For comparison, an argon-ion laser has a bandwidth of < *0.0001 nm*, while a free running excimer laser has a bandwidth of *1nm*. In lithography applications, excimer sources are often line narrowed to a few picometers, but are still much broader than an argon-ion laser [39,40]. Probably a better result would be obtained by excimer lasers.

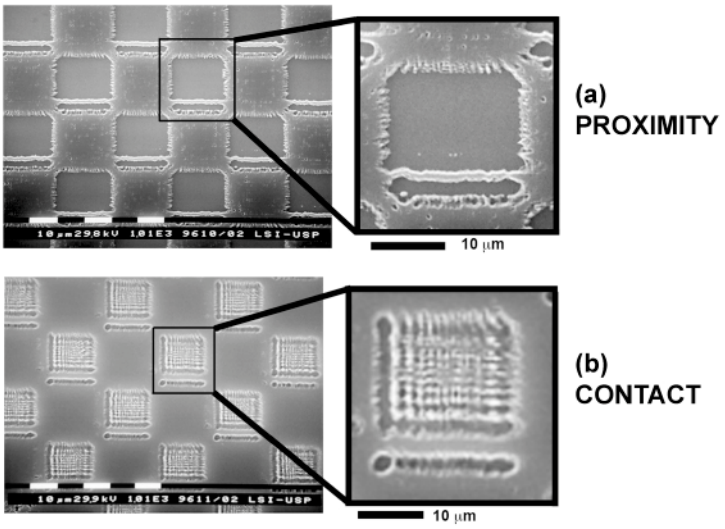

Fig. 12. SEM images of the resulting structures from the two kind of exposures. (a) proximity printing mode and (b) contact printing mode. The structures obtained from the proximity mode are much better defined.

A second test was performed by using extended, partially coherent UV light in the exposure. In this case, an i-line filter was used to remove all wavelengths but the i-line from a small mercury light source. Although the mask was designed to operate with coherent light, there is a coherence length below which the exposure can be considered quasi coherent. This behaviour allows us to explore the partiall coherence of light. The coherence length is given by the Van Cittert-Zernike theorem [41–44]. This theorem establishes the condition of a system illuminated by a polychromatic extended source to be considered in a partial coherent regime of operation.

Consider light emerging from an extended polychromatic source of size ρ, with mean wavelength, $\bar{\lambda}$, illuminating a plane at a distance R from the source.

The regime of partial coherence can be achieved if the distances involved in the system obey the following relation:

$$d\left(P_1, P_2\right) = \frac{0.16R\bar{\lambda}}{\rho} \tag{18}$$

where $d(P_1,P_2)$ is the distance between two adjacent points belonging to a wavefront.

In order to maximize the coherence length one has to: i) make exposure with a light source as far as possible, and/or ii) employ a light source with wavelength as long as possible, and/or iii) use a light source with extension as small as possible.

#130279 - $15.00 USD Received 17 Jun 2010; revised 6 Jul 2010; accepted 7 Jul 2010; published 20 Jul 2010

In our exposure tool, the distance $R = 1.5\ m$ and $\bar{\lambda} = 365\ nm$. The extension of the source is the linear dimension of mercury arc lamp used, hence $\rho = 2\ mm$. Using the values above, the coherence length equals to $d(P_1,P_2) = (0.16 \times 1.5 \times 365 \times 10^{-9}) / 2\ 10^{-3} = 43.8\ \mu m$.

This dimension is larger than the squares of the test structures of Fig. 12 (*20* by *20 μm* squares), enabling a locally quasi coherent regime.

Figure 13 shows the comparative results for partial coherent illumination. In this case, exposures in contact (Fig. 13a), proximity with *50 μm* gap (Fig. 13b), and proximity with 100 μm gap (Fig. 13c) were performed. One can observe again the necessary condition of a *50 μm* gap in order to obtain better resolution. Both contact mode and proximity with a *100 μm* gap result in poorer resolution with respect to the *50 μm* gap exposure. Besides, the speckle noise was eliminated since in this case a partially coherent regime was used.

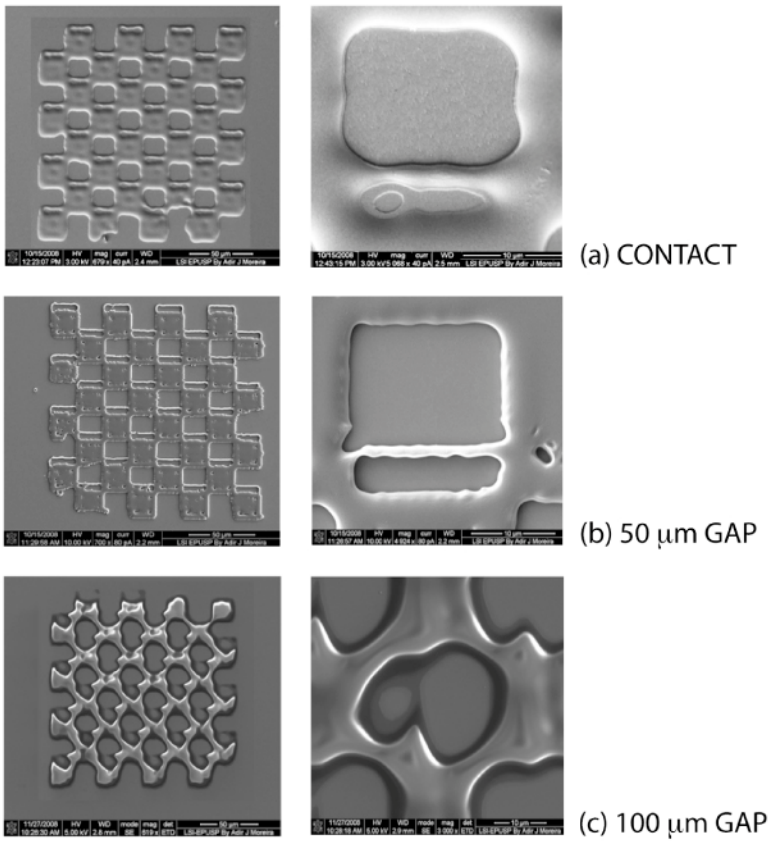

Fig. 13. SEM micrographs of the resulting structures obtained by using a partially coherent light source. (a) contact exposure. (b) 50 μm gap proximity exposure; (c) 100 μm gap proximity exposure.

Figure 14 shows part of the test structures with a detail of a line *1.5 μm* wide by *82 μm* length, patterned in proximity (*50 μm* gap) and contact modes. One can note that the line obtained by proximity exposure is clearly resolved while that obtained by contact exposure is barely resolved.

#130279 - $15.00 USD Received 17 Jun 2010; revised 6 Jul 2010; accepted 7 Jul 2010; published 20 Jul 2010

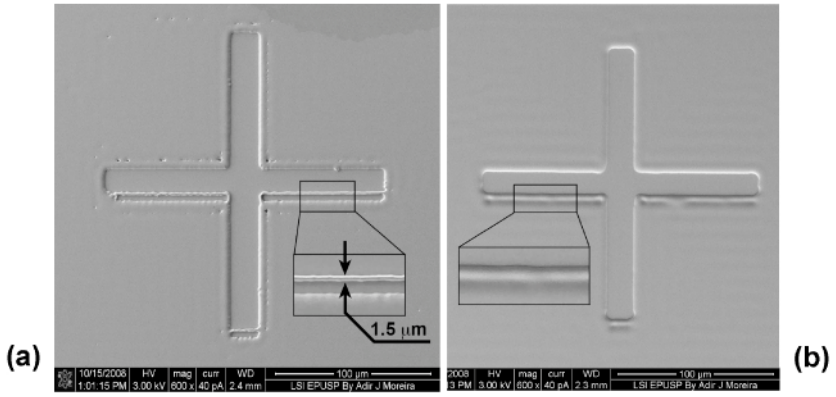

Fig. 14. SEM micrographs of part of the test structures with a detail of a line 1.5 μm wide by 82 μm length, patterned in (a) proximity (50 μm gap) and (b) contact modes. The line obtained by proximity exposure is clearly resolved while that obtained by contact exposure is barely resolved.

5. Conclusions

We designed, fabricated and tested a phase shift diffractive photomask, which operates in the proximity printing regime, forming the required image at a predetermined distance of *50 μm* behind the mask. This mask was fabricated using an amorphous hydrogenated carbon (a:C-H) thin film on top of a patterned fused silica substrate. The fused silica is used to modulate the phase and the a:C-H layer to modulate the amplitude of the incoming UV light (*365 nm* wavelength). The first important feature of the proposed mask is that the resolution can be improved by the compensation of diffraction effects when compared to a conventional (binary, amplitude only) photomask. The results show a resolution as good as *1.5 μm*, what is impossible with traditional diffraction-uncompensated binary masks in proximity printing mode.

The pattern transfer to a fused silica substrate by reactive ion etching based on CF_4 chemistry presents some imperfections, mainly at the edges of the structures. In future works we want to optimize the fidelity of the pattern transfer to fused silica, with low induced line edge roughness. Despite this induced roughness, it was possible to demonstrate the proposed principle of exploring the diffraction of light along the *50 μm* gap between mask and wafer.

Although the resolution achieved by this technique is far larger for today's microelectronic devices fabrication, it is still very suitable for MEMS and MOEMS applications, with dimensions that typically range from several micrometers to several millimeters.

The second important feature of the proposed mask is that the a:C-H film is partially transparent in the visible region, helping the alignment of subsequent lithographic masks during MEMS/MOEMS devices fabrication, reducing its processing time.

Two types of light source were used to expose photoresist: an argon ion laser and also a small UV lamp where the illumination system operates in partial coherence regime. A comparative result showed that the resolution of a test structure exposed with the proposed mask was far better in proximity mode than those exposed in contact mode, when keeping all the other process parameters the same. The laser source resulted in a pattern affected by speckle noise, while the arc lamp source eliminated this effect.

Acknowledgment

The authors would like to thank CTI for the fabrication of the photolithographic masks, and the agencies Conselho Nacional de Desenvolvimento Cientfico e Tecnológico (CNPq), process # 151908/2007-9, and Fundação de Amparo à Pesquisa no Estado de São Paulo (FAPESP), processeses # 00/10181-2 and # 00/11117-6. This work is part of the Instituto

Nacional de Ciência e Tecnologia: Óptica e Fotônica (INCT-INOF), sponsored by CNPq (process # 573587/2008-6) and FAPESP (process # 08/57858-9).

#130279 - $15.00 USD Received 17 Jun 2010; revised 6 Jul 2010; accepted 7 Jul 2010; published 20 Jul 2010